Mineralogia, vol. 53, 2022, 51-66 *Original Paper*

DOI: 10.2478/mipo-2022-0005

MinPlot: A mineral formula recalculation and plotting program for electron probe microanalysis

Jesse B. Walters*

Institut fûr Geowissenschaften, Goethe Universität, Frankfurt am Main, 61348
*Corresponding author: thegeojesse@gmail.com

Abstract

MinPlot is a MATLAB®-based mineral formula recalculation and compositional plotting program for electron microprobe analyses (EPMA). The program offers recalculation and structural formula assignment for 15 different mineral groups: Garnet, pyroxene, olivine, amphibole, feldspar, mica, staurolite, cordierite, chlorite, chloritoid, talc, epidote, titanite, spinel, and sulfides. MinPlot is a fast and easy to use command line program and requires no prior computer programming knowledge. Percent mass fractions of oxides are loaded from datafiles and the user answers simple prompts to select mineral type, normalization scheme, and plotting options. Recalculated mineral formulas are automatically saved as output files and plots may be further manually customized by the user prior to saving. MinPlot can perform thousands of calculations in seconds and the modular nature of the program makes it simple to add new calculation routines in future releases. Combined, these features make MinPlot a powerful and useful program for the processing of EPMA data.

Keywords: Melectron microprobe, structural formula, plotting, computer program, mineral chemistry

1. Introduction

Electron probe microanalysis (EPMA) is one of the most powerful and commonly used tools for the quantitative determination of mineral compositions. Following analysis, standardization, and corrections for atomic number, absorption, and fluorescence effects, data are reported by the EPMA software as the percent mass fraction (g/g × 100) of oxides (e.g., SiO_2, TiO_2, Al_2O_3, etc) or elements (e.g., Si, Ti, Al, etc). Conversion to the atomic proportions of the mineral formula is necessary for mineral classification and assessment of compositional trends, such as changes of endmember fractions in zoned minerals. Over the years many programs have been offered which convert percent mass fraction of oxides to mineral structural formulae for specific minerals, such as garnet (Grew et al. 2013; Knowles 1987; Locock 2008; Yavuz, Yildirim 2020), pyroxene (Sturm 2002; Yavuz 2013), mica

© Author(s) 2022. This work is distributed under the Creative Commons BY 4.0 license (https://creativecommons.org/licenses/by/4.0/)

(Yavus 2003a, b), chlorite (Yavuz et al. 2015), amphibole (Locock 2013; Esawi 2004; Mogessie et al. 1990; Mogessie 2001; Rao, Rao 1996; Richard, Clark 1990; Rock 1987; Rock, Leake 1984; Spear, Kimball 1984; Tindle, Webb 1994; Yavuz 2007), and others. Other programs allow for the recalculation of formulae for a variety of mineral species: MINFILE (Afifi, Essene 1988), MINTAB (Rock, Caroll 1990), HYPER-FORM (De Bjerg et al. 1992), PASFORM (De Bjerg et al. 1995), CALCMIN (Brandelik 2009), MINCALC (Bernhard 2010), and MINERAL (De Angelis, Neill 2012). While there are many available programs offered over the years, all established programs have restrictions limiting or entirely preventing their use on modern computing operating systems. Many of these, such as MINCALC, CALCMIN, WinAmphcal, and others, utilize the Visual Basic programming language coupled with Microsoft Excel™; however, the Visual Basic language was abandoned by Microsoft© and these programs may no longer function. Additionally, Visual Basic-based programs can only be operated on Windows™ systems, requiring users of other operating systems to run virtual machines. MINERAL (De Angelis, Neill 2012) is a powerful MATLAB®-based program which calculates mineral formulae with error propagation, and can recalculate the formulae of feldspar, olivine, pyroxene, spinel, ilmenite, amphibole, garnet, epidote, and mica. While Fe^{3+}-Fe^{2+} estimation is calculated in MINERAL, normalization to 15 or 13 cations for amphibole is only appropriate for some compositions (Leake et al. 1997; Hawthorne et al. 2012). XMapTools offers both mineral structural formula recalculation as well as plotting but is specialized for quantitative mapping by EPMA and LA-ICP-MS (Lanari et al. 2014a; 2019). However, no program offers options for both automated publication-ready plotting and mineral formula recalculation for standard EPMA point analysis.

Here a new MATLAB®-based command line program, called MinPlot, is presented. MinPlot can perform mineral formula recalculation and automated compositional plotting for garnet, pyroxene, olivine, amphibole, feldspar, mica, staurolite, cordierite, chlorite, chloritoid, talc, epidote, titanite, spinel, and sulfides. Users need no programming experience and MinPlot is functional on any computer capable of running MATLAB®. Importantly, the program offers a flexible approach, with multiple yes-no prompts, allowing the user to choose multiple normalization and plotting schemes where appropriate. Unlike spreadsheet-based approaches, MinPlot can calculate recalculate hundreds to thousands of analyses within seconds. The program is capable of outputting publication-ready compositional diagrams that are commonly used in the literature. The modular approach to the program, which runs on from a central script that calls functions for each mineral, means that the addition of new minerals or normalization procedures in the future requires little modification of the existing programming framework. Finally, the MATLAB® language is forwards compatible and the program will continue to function in the future as the language is updated.

2. Program Design

2.1. General Formula Recalculation Procedure

MinPlot is based around a central script (MinPlot.m), which calls functions for each mineral (e.g., garnet_fe3.m, garnet_fe2.m, etc). Mineral functions differ in their design and complexity, with only a single function for minerals like feldspar and epidote, and up to twelve functions for amphibole. The same basic formula is applied, in linear programming steps, to calculate molar proportions of cations and oxygens, respectively, from the mass fraction of the oxides:

$$n_i^C = \frac{w_j}{m_j} \cdot M_j^C \tag{1}$$

and

$$n_i^O = n_i^C \cdot \frac{M_j^O}{M_j^C} \tag{2}$$

Where n_i^C and n_i^O are the unnormalized moles of cations and O, respectively, of element *i* in the analyzed phase, W_j is the measured mass fraction of the oxide *j* (in weight percent), m_j is the molecular weight of the oxide *j*, and M_j^C and M_j^O are the moles of cations and O, respectively, in the oxide *j*. Molecular weights of the oxides are calculated using the atomic weights using the values reported in the *Atomic weights of the elements 2013 (IUPAC Technical Report)* of Meija et al. (2013).

Calculation of the atoms per formula unit (APFU) of each element and their assignment in the structural formula of the mineral follow a normalization procedure based on assumptions of charge balance. While the normalization procedure is specific to each phase, it may generally be summed up as shown in the following. Normalization on an oxygen equivalents basis for some minerals (assuming a fixed number of negative charges) is calculated following Equation 3:

$$NF^O = \frac{n_{ideal}^O}{\sum_i^Z n_i^O} \tag{3}$$

Where NF^0 is the oxygen-based normalization factor, Z is the number of elements, and n_{ideal}^O is the ideal moles of oxygen (negative charges) per formula unit (e.g., 12 for garnet, 4 for olivine, 6 for pyroxene, etc). For Cl and F-bearing minerals, the sum of the negative charges ($\sum_i^Z n_i^O$) is adjusted by subtracting one-half the moles

of F + Cl. For some hydrous phases, such as mica, amphibole, and staurolite, OH content is calculated as the ideal minus F + Cl. Normalization is conducted over 50 iterations until stable normalization factors are converged upon.

Normalization of garnet, olivine, pyroxene, spinel, and chloritoid uses the method of Schumacher (1991) for Fe^{3+}-Fe^{2+} calculation. Prior to Fe^{3+} estimation, the moles of cations are normalized on a cation basis (assuming a fixed number of positive charges):

$$NF^C = \frac{n^C_{ideal}}{\sum^Z_i n^C_i} \quad (4)$$

Where NF^C is the cation-based normalization factor and n^C_{ideal} is the ideal moles of cations (positive charges) per formula unit (e.g., 8 for garnet, 3 for olivine, 4 for pyroxene, etc). For some minerals, such as amphibole, Z is less than the total number of elements and is less than an ideal the sum of all the cations. In these cases, the normalization procedure assumes that only certain sites are full and is useful for minerals with structural vacancies. Once the correct normalization procedure is made, the unnormalized moles of cations are multiplied by the normalization factor:

$$n^{Norm}_i = n^C_i \cdot NF^C \quad (5a)$$

or

$$n^{Norm}_i = n^C_i \cdot NF^O \quad (5b)$$

Where n^{Norm}_i is the normalized moles of each cation (in APFU).

Ferric iron calculation follows Schumacher (1991) for garnet, olivine, pyroxene, spinel, and chloritoid. In these cases, the oxygen sum ($\sum^Z_i n^O_i$) is calculated using the moles of oxygen calculated by Equation 2 following normalization using Equation 5 on a cation basis. The oxygen, or rather charge, deficiency determines the amount of Fe calculated as Fe^{3+}:

$$OD = n^O_{ideal} - \left(\sum^Z_i n^O_i\right)_{\text{cation normalized}} \quad (6)$$

Where *OD* (oxygen deficiency) must be greater than 1 to calculate Fe^{3+} using charge balance constraints. The amount of Fe^{3+} and Fe^{2+} are calculated as:

$$n^{norm}_{Fe^{3+}} = 2 \cdot OD \quad (7a)$$

And

$$n^{norm}_{Fe^{2+}} = n^{norm}_{Fe} - n^{norm}_{Fe^{3+}} \quad (7b)$$

Where $n^{norm}_{Fe^{2+}}$ and $n^{norm}_{Fe^{3+}}$ are the moles of Fe^{3+} and Fe^{2+} in atoms per formula unit, respectively. If $n^{norm}_{Fe} > 2 \cdot OD$, then $n^{norm}_{Fe^{3+}}$ is assumed to equal n^{norm}_{Fe} ($Fe^{3+}/\Sigma Fe = 1.0$), otherwise MinPlot automatically calculates $n^{norm}_{Fe^{3+}} = 0$ if $2 \cdot OD \leq 0$. The oxygen deficiency is output with the structural formula and analyses with negative OD values should not be considered if Fe^{3+} estimation is important. Formula recalculation assuming $\Sigma Fe = Fe^{2+}$ are also available for garnet, pyroxene, and olivine.

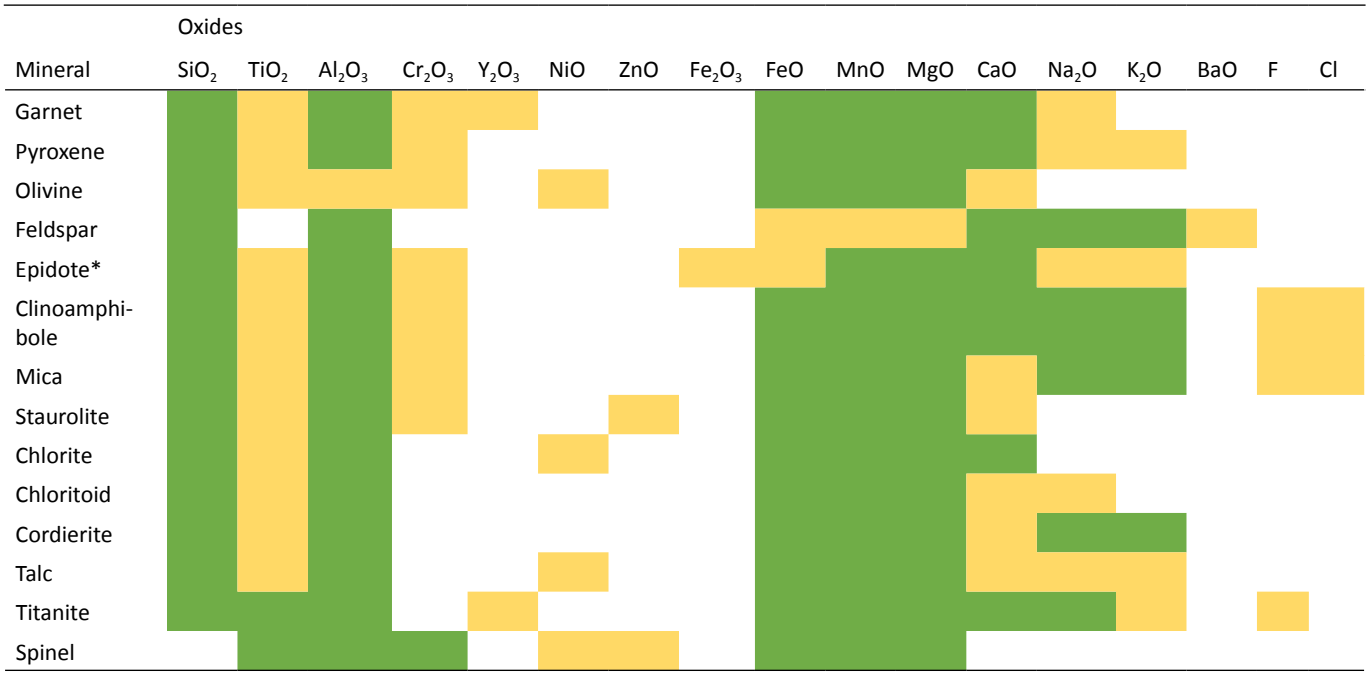
2.2. General approach to structural formula assignment

Site assignment to the structural formula follows the standard procedure of filling the structurally smallest sites first, such as the tetrahedral site in silicate phases. The tetrahedral sites are not allowed to contain excess Si. For example, if the calculated Si content (APFU) in garnet is less than 3, then the calculated value is used; however, if Si is in excess, then a value of 3 is assigned. ^{VI}Al is then assigned: If the tetrahedral site is full, all Al is treated as ^{VI}Al, otherwise some ^{IV}Al may be assigned. For low Al garnets, such as andradite, all Al could theoretically be ^{VI}Al. If 3 - Si is greater than the calculated Al content (APFU), then all Al is assumed to be Al^{IV}, otherwise $^{IV}Al = 3 - Si$. Ferric iron may also be assigned to the tetrahedral site if the site is not already filled by Al + Si. Assignment of Al to structurally larger sites, such as the octahedral site in garnet, is calculated as Al_{total}-^{IV}Al. A similar calculation is done if ferric iron is partially assigned to the tetrahedral site. This procedure, with or without ferric iron, is followed for tetrahedral site assignment in all silicate phases. Assignment to structurally larger sites in most silicate phases follows a more straightforward procedure, e.g. all Ca in garnet is assigned to the dodecahedral site, and maximum site assignments are not imposed. The sum of the site occupancies should be checked by the user to ensure the quality of the analysis. Most structural assignments do not assume equipartitioning, except for pyroxene. The order and method of site assignment for specific phases is given in the scripts for each phase, with worked examples for each phase given in Table S1.

2.3. Loading and Saving Data

MinPlot reads data stored as text (.txt) files. The first line must contain oxide-based headers that are specific to the mineral formula to be recalculated (see Table 1). The headers must have capital and lowercase characters as shown in Table 1. For some phases, certain oxides are optional and will be calculated assuming a mass fraction of zero ($W_j = 0$) if they are not included in the file read by MinPlot. MinPlot searches the header row for the column containing the appropriate header for each oxide, as a result the oxide data can be listed in any order in the input file. To start MinPlot, change the MATLAB® directory to the folder containing MinPlot and type the

Table 1. The following oxides (in wt. %) are either required (green) or optional (yellow) in the data file read by MinPlot.



*Need to include either FeO or Fe_2O_3, not both.

name of the program into the command window and hit the 'return' key. When loading the data, the user is prompted to select the file in a pop-up window and, importantly, the file can be located in any folder on the user's computer or in their network. Following calculation, the user is prompted to save their calculation. If yes, the data is automatically saved as tab delimited text files in the same directory as the source file, allowing for simplified data organization.

2.4. Plotting Data

Automated plotting of compositional data is available for most minerals and the user may select which types of plots they want to make for the mineral of interest. A select set of options are available for symbol type (circle, square, diamond, triangle), color (blue, orange, yellow, purple, green, cyan, and red), and symbol size (a non-dimensional scalar value, input values between 50-200 are appropriate for most practical applications). Plots are not automatically saved. Instead, the variety of potential file types (e.g., .pdf, .png, .jpg, etc), degree of compression, manual modification the figure prior to saving (e.g., adjustment of colors, widths, etc), and choice of a vector- or raster-based image format, offered by MATLAB® give the user more flexibility when saving plots manually. For example, saving plots as a vector-based PDF allows the user to modify the plots in a vector graphics editor program prior to publication.

3. Calculation and Plotting Routines

Below the mineral-specific recalculation procedures and plotting are described. Note that all plots are resized by 50 to 60% and the font is changed to match journal specifications; however, the plots are otherwise unchanged from the MinPlot output. Tables of worked examples of literature data recalculated in MinPlot are given in supplementary Table S1. All mineral abbreviations are after Warr (2021), except where noted.

3.1. Garnet Supergroup

Garnet ($X_3Y_2Z_3O_{12}$) has a flexible structure and can incorporate a variety of elements in its four crystallographic sites (Grew et al. 2013). Here the compositional space is restricted to those elements which are abundant in most natural garnets and can be measured on the EPMA: X = Na, Ca, Mg, Mn, Fe^{2+}, and Y at the dodecahedral site, Y = Fe^{2+}, Mg, Mn, Fe^{3+}, Cr, Ti, ^{VI}Al, and excess Si at the octahedral site, Z = Fe^{3+}, ^{IV}Al, and Si at the tetrahedral site, and O_2 at the anion site. The hydrogarnet substitution, $4H + {}^{z}\square \rightarrow \square + {}^{z}Si$, may be significant in garnets along the grossular-katoite join but is not considered here. Garnet structural formula are calculated using normalization to 8 cations and 12 oxygens (for Fe^{3+}-estimation), or 12 oxygen basis alone (for ΣFe = Fe^{2+}). Endmember fractions are calculated using the matrix inversion method for solving systems of linear equations:

$$X_{Endmembers} = M^{-1} \cdot A_T \quad (8)$$

Where $X_{Endmembers}$ is the matrix of endmember fractions, M^{-1} is a matrix of the ideal moles of the cations for each endmember, and A_T is the transposed matrix of Ca, Mg,

ΣFe, Cr, Mn, and Al cations for each analysis. Following Equation 8, the sum of the endmembers is calculated and normalized to unity. Equation 8 is convenient for rapidly solving large systems of linear equations; however, only square matrices are invertible, and the technique is not appropriate for all endmember calculations. The garnet endmembers considered are almandine (X_{alm}), spessartine (X_{sps}), grossular (X_{grs}), pyrope (X_{prp}), andradite (X_{adr}), and uvarovite (X_{uv}).

Plotting options for garnet include the X_{alm} + $X_{sps,}$ $X_{grs,}$ and X_{prp} ternary (Fig. 1a). It is important to note that X_{sps} and X_{alm} do not perfectly co-vary, especially at low pressure and temperature conditions near the garnet-in reaction (e.g., Caddick, Kohn 2013), and restricting the 4-dimensional endmember composition space of common garnets to 3-dimensions will obscure compositional trends. A second Fe^{3+}, Cr + Ti, and ^{VI}Al ternary diagram for substitutions at the octahedral site is also available (Fig. 1b).

3.2. Pyroxene

Pyroxene ($M2M1T_2O_6$) compositions are calculated following Morimoto et al. (1989), with K, Na, Ca, Fe^{2+}, and Mg at the distorted octahedral M2 site, Fe^{2+}, Mg, Mn, Cr, Fe^{3+}, Ti, and ^{VI}Al at the octahedral M1 site, and Fe^{3+}, ^{IV}Al, and Si at the tetrahedral site. Vanadium, Zn, and Sc may also substitute at the M1 site, but are typically observed at trace levels, whereas Li may substitute at M2 as a major element in spodumene but is not measurable by EPMA. These elements are not considered here. Ferrous iron and Mg are equipartitioned between M1 and M2 sites. Normalization is to 4 cations and 6 oxygens in the Fe^{3+}-estimation routine, and on a 6-oxygen basis for ΣFe = Fe^{2+}. Endmember fractions are calculated using Equation 8 for wollastonite (X_{wo}), ferrosillite (X_{fs}), enstatite (X_{en}), jadeite (X_{jd}), aegirine (X_{aeg}), and kosmochlore (X_{kos}). In high pressure and/or temperature pyroxenes, the potassium clinopyroxene ($KAlSiO_2O_6$ and $KCrSi_2O_6$), calcium-Eskola ($Ca_{0.5}AlSi_2O_6$), and calcium-Tschermaks ($CaAlAlSiO_6$) components may significant (Harlow 1999). An optional pyroxene endmember calculation is also provided and follows the procedure of Harlow (1999), where endmembers are calculated as jadeite (X_{jd}), aegirine (X_{aeg}), diopside + hedenbergite (X_{di+hd}), calcium-Tschermaks pyroxene (X_{cats}), kosmochlor (X_{kos}), K-kosmochlor ($X_{K\text{-}kos}$), K-jadeite ($X_{K\text{-}jd}$), calcium-Eskola pyroxene (X_{caes}), and enstatite (X_{en}). Abbreviations for calcium-Tschermaks and calcium-Eskola pyroxene are also after Harlow (1999).

Plotting and classification also follows Morimoto et al. (1989). First, the so called 'Q-J' diagram distinguishes Ca-Mg-Fe pyroxenes (Quad), Na-Ca pyroxenes (Na-Ca), and Na pyroxenes (Na), where J = 2Na is plotted on the x-axis and Q = Ca + Mg + Fe^{2+} is plotted on the y-axis (see Fig. S1). For Ca-rich pyroxenes, the user may restrict endmember calculation and plotting to 'Quad' compositions, which is a useful approximation for many igneous pyroxenes. Discrimination plots also include the X_{wo}, X_{fs}, and X_{en}, (Fig. 2a) and X_{quad}, X_{jd}, and X_{aeg} (Fig. 2b) ternaries after Morimoto et al. (1989). Plots of X_{caes} and X_{cats} and $X_{K\text{-}cpx}$ ($X_{K\text{-}cpx} = X_{K\text{-}kos} + X_{K\text{-}jd}$) and X_{caes} following Harlow (1999) are also available (Fig. S2).

3.3. Olivine

Olivine (M_2TO_4) is calculated here with M = Ca, Mg, Mn, Fe^{2+}, Ni, Cr, Fe^{3+}, Ti, and ^{VI}Al at the octahedral site, and T = Fe^{3+}, ^{IV}Al, and Si at the tetrahedral site. Normalization

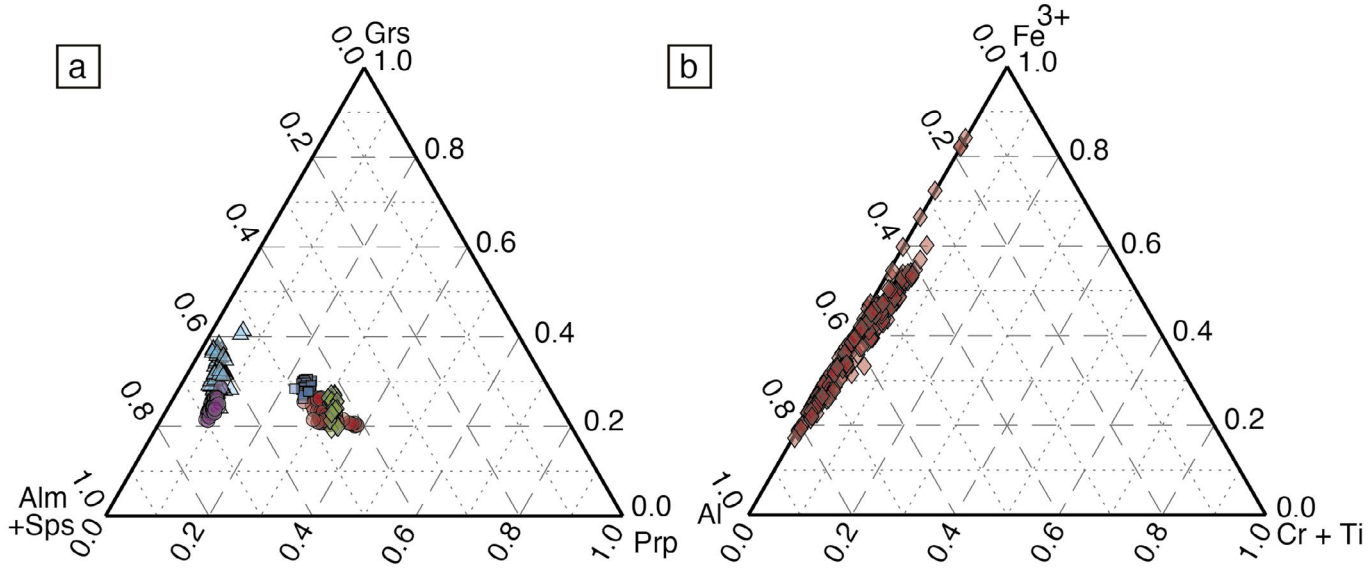


Figure 1. (a) Ternary grossular, almandine + spessartine, and pyrope, and (b) Fe^{3+}, Al, and Cr + Ti garnet compositional diagrams. Example garnet for (a) data are from Walters et al. (2019; 2021): Light blue triangles – garnet blueschist (DR1203-11-03; Dominican Republic), purple circles – garnet-omphacite-chlorite fels (SY462; Syros, Greece), red circles – metagabbroic eclogite (G083-12; Vendée, France), dark blue squares – eclogite (SVS-11-01; Svetlik-Sus, Czech Republic), and green diamonds – eclogite (TIS-11-02; Tisova, Czech Republic). Example data for (b) (red diamonds) were collected on grossular-andradite skarn garnet from Xanthi, Greece (Unpublished).

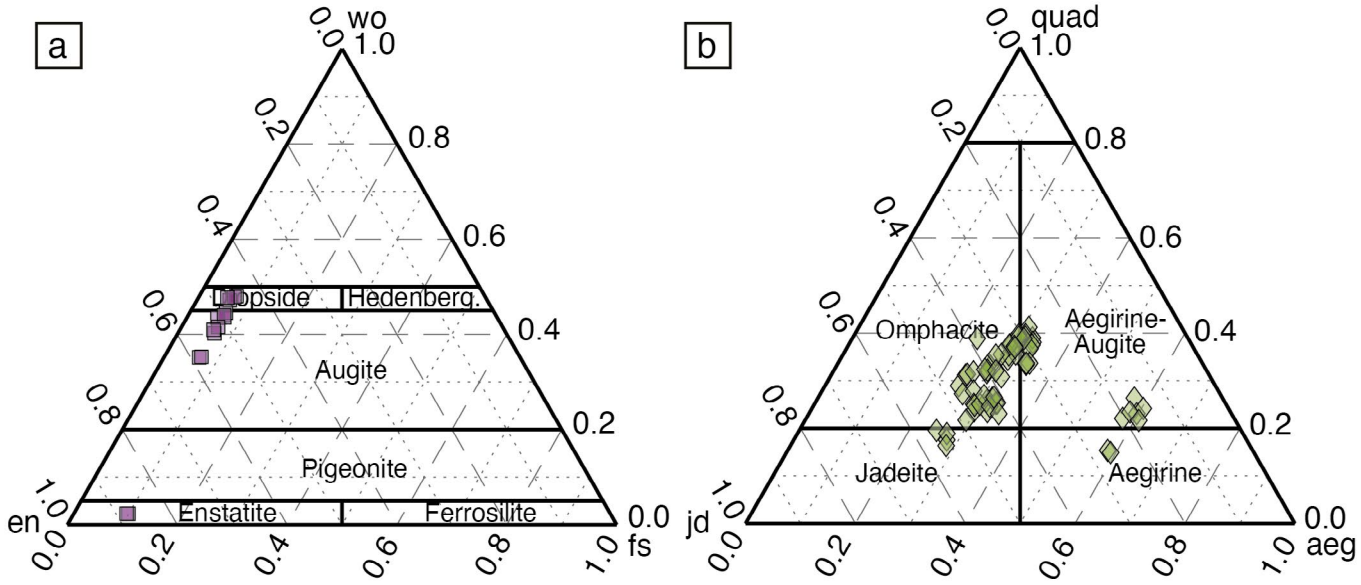


Figure 2. (a) Ternary wollastonite, enstatite, and ferrosilite, and (b) quad., jadeite, and aegirine pyroxene compositional diagrams. Example data in (a) are clino- and orthopyroxene grains from gabbro-norite cumulate bodies and dikes from Alpine-Apennine ophiolites (Piccardo, Guarnieri 2011). Example data in (b) are Na-clinopyroxene from a metasomatic garnet-omphacite-chlorite fels from Syros, Greece (SY462; Walters et al. 2019; 2021).

is to 3 cations and 4 oxygens in the Fe^{3+}-estimation routine, and on a 4-oxygen basis for ΣFe = Fe^{2+}. Endmember fractions are calculated using Equation 8 for forsterite (X_{fo}), fayalite (X_{fa}), tephroite (X_{te}), and calcio-olivine ($X_{Ca\text{-}ol}$). Three plots are available for olivine (Fig. 3). First is an option for a binary plot of the forsterite content (Fig. 3a), where the user is prompted to specify the upper and lower Fo limits. Second, a ternary diagram in the X_{fo}, $X_{Ca\text{-}ol}$, and X_{fa} + X_{te} system is available (Fig. 3b). Finally, a plot with the Fo number on the x-axis and mass fraction of NiO (wt%) on the y-axis is available (Fig. 3c).

3.4. Amphibole Supergroup

Amphibole ($AB_2C_5T_8O_{22}W_2$) has a complex structure with a wide compositional space. MinPlot follows the recommendations of Leake et al. (1997) and Hawthorne et al. (2012) for structural assignment, with A = □, K, Na, and Ca at the *A* site, B = Ca, Na, Mn, Fe^{2+}, and Mg at the *M*4 site, C = Mn, Fe^{2+}, Mg, Fe^{3+}, Cr, Ti, and Al at the *M*1, *M*3, and *M*2 sites, T = Si and Al at the *T* site, and OH^-, F^-, Cl^-, and O^{2-} at the *W* site. Minor elements, such as Pb, Zn, Co, V, Sc, and Zr, typically have contents at or below the

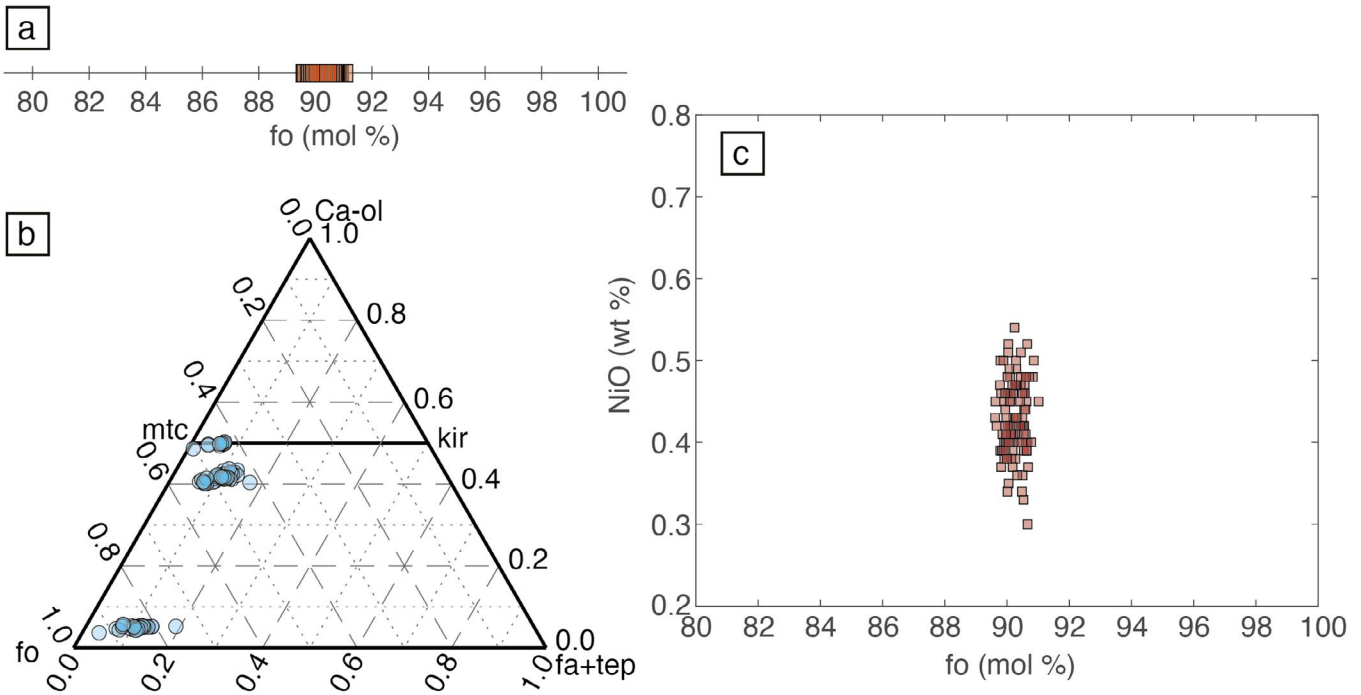


Figure 3. (a) Binary forsterite, (b) ternary forsterite, calcio-olivine, and fayalite + tephroite, and (c) forsterite vs. NiO (wt%) olivine compositional diagrams. Data in (a) and (c) are analyses of olivine from mantle peridotite, Wadi Fins, Oman (de Obseso, Kelemen 2020). Data in (b) are analyses of experimentally grown olivine (Le Pioufle, Canil 2012).

EPMA detection limit and are not included. Additionally, Li and Be cannot be measured by EPMA and are also excluded. For a more complete formula recalculation and classification of amphiboles, including Li and other minor elements, see Locock (2014).

Amphibole formula recalculation presents multiple challenges, particularly estimation of Fe^{3+}-Fe^{2+} and the occupancy of the *W*-site. The calculation procedure here follows the IMA recommendations of Hawthorne et al. (2012) and iterative OH estimation is based on Locock (2014). The procedure is summarized here. Amphibole is commonly normalized on the basis of 24(O,OH,F,Cl) where occupancy of the *W*-site is ^{W}(OH,F,Cl) = 2 APFU, therefore if H_2O is not analyzed the normalization is based on 23 oxygen equivalents (anhydrous basis). However, substitution of Ti in the *M*1 site is commonly balanced by incorporation of O^{2-} (Oberti et al. 1992):

$$^{C}R^{2+} + 2^{W}(OH)^{-} \rightarrow {}^{C}Ti^{4+} + 2^{W}O^{2-} \quad (9)$$

As a result, ^{W}(OH,F,Cl) can be calculated as (2 - 2Ti) APFU, thus correcting for the maximum possible contribution of O^{2-} at the *W*-site (Hawthorne et al. 2012). This assumes that Ti_{M3} and Ti_{M2} are negligible, which is not always the case (see Tiepolo et al. 1999). MinPlot allows the user to choose formula recalculation assuming ^{W}(OH,F,Cl) = 2 APFU (23 oxygen equivalents) or with the Ti-O^{2-} correction. For the Ti-O^{2-} correction, the normalization factor is >23 oxygen equivalents and adjusted using the Ti content based on Equation 9.

Ferric iron estimation can be calculated through normalization to sets of cation sums which provide lower and upper $Fe^{3+}/\Sigma Fe$ limits (Leake et al. 1997; Hawthorne et al. 2012). It is important to note that stoichiometric estimation of Fe^{3+}-Fe^{2+} requires all major cations to be analyzed and is thus not appropriate here for Li-rich compositions. Additionally, Fe^{3+} may be charge balanced by dehydrogenation, which is not considered in MinPlot. The Fe^{3+}-Fe^{2+} calculation procedure is as follows. First, the all-ferrous formula is calculated to give the maximum number of cations. Lower $Fe^{3+}/\Sigma Fe$ limits are calculated from the all-ferrous formula based on the three following criteria:

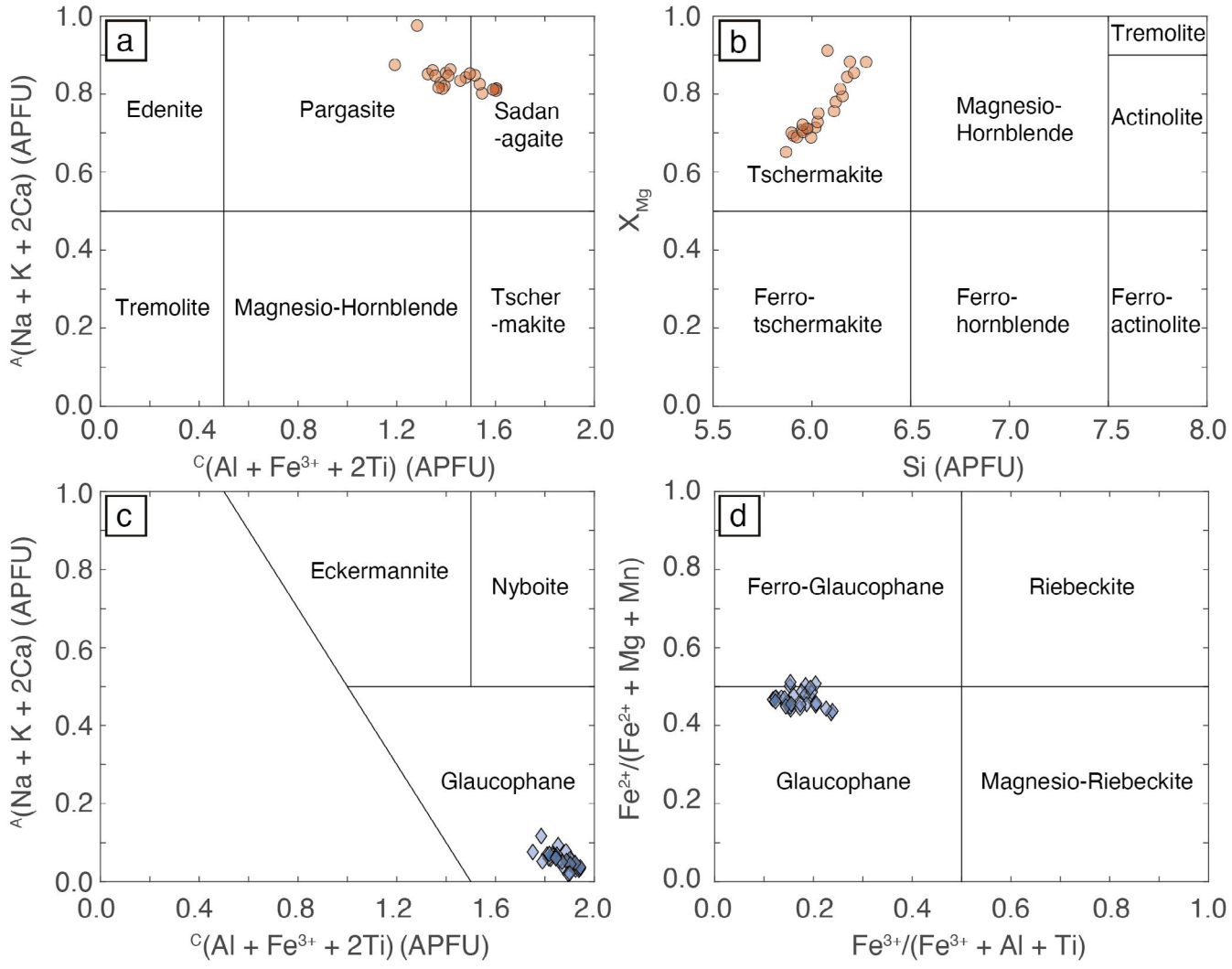


Figure 4. Clinoamphibole compositional and classification diagrams (after Hawthorne et al. 2012; Leake et al. 1997): (a) ^{C}(Al + Fe^{3+} + 2Ti) vs ^{A}(Na + K + 2Ca) diagram for Ca-amphibole, (b) Si vs X_{Mg} diagram for Ca-Amphibole, (c) ^{C}(Al + Fe^{3+} + 2Ti) vs ^{A}(Na + K + 2Ca) diagram for Na-amphibole, and (d) $Fe^{3+}/(Fe^{3+}$ + Al + Ti) vs $Fe^{2+}/(Fe^{2+}$ + Mg + Mn) diagram for Na-amphibole. Analyses of glaucophane are collected on blueschists from Port Macquarie, Australia (PMQ065). Ca-amphibole analyses are collected on zoned amphibole from a retrogressed eclogite from Svetlik-Sus, Czech Republic (SVS-11-01; Walters et al. 2019; 2021).

(1-1) Si ≤ 8 APFU
(1-2) (Si + Al + Ti +Cr + Fe^{2+} + Fe^{3+} + Mn + Mg + Ca + Na+ K) ≤ 16 APFU
(1-3) (Si + Al + Ti +Cr + Fe^{2+} + Fe^{3+} + Mn + Mg + Ca) ≤ 15 APFU

Criteria 1-1 and 1-2 are set by the structure. There cannot be more than 8 Si cations on the *T* site or 16 total cations. Criterion 1-3 assumes that Ca does not incorporate into the *A*-site, which may not be true in amphiboles from Ca-rich rocks, like marbles and calc-silicates (Hawthorne et al. 2012). If none of these criteria are invalidated, the minimum Fe^{3+} estimate comes from the all-ferrous formula. The upper $Fe^{3+}/\Sigma Fe$ limits are calculated using the five following criteria:

(2-1) (Si + Al) = 8 APFU
(2-2) (Si + Al + Ti +Cr + Fe^{2+} + Fe^{3+} + Mn + Mg + Ca + Na) = 15 APFU
(2-3) (Si + Al + Ti +Cr + Fe^{2+} + Fe^{3+} + Mn + Mg) = 13 APFU
(2-4) (Si + Al + Ti + Cr + Fe^{3+}) = 10 APFU
(2-5) ΣFe = Fe^{3+}

Criterion 2-1 assumes that Si and Al only substitute at the tetrahedral site; whereas, criterion 2-2 assumes that only K substitutes at the *A* site. Hawthorne et al. (2012) warn that criteria 2-1 and 2-2 are not appropriate for high-temperature richterite compositions where Ti may occur as a T cation and K may occur as a B cation. It is important to note that the estimation schemes here will not explicitly yield the Ti and K occupancies needed to identify this composition, and caution must be taken if this composition is suspected. Additionally, criterion 2-2 is inappropriate for amphiboles with an edenite ($NaCa_2Mg_5(Si_7Al)O_{22}(OH)_2$) component, such as hornblende, as it assumes Na is not an A cation. Criterion 2-3 assumes that C = Fe^{2+}, Mn, or Mg, which may be violated if these elements also substitute for B group cations. Criterion 2-4 assumes that 3+ and 4+ cations fill the *T* and *M*2 sites, and the normalization factor is calculated as 36/(46-Si-Ti-Al-Cr) (Leake et al. 1997). Criterion 2-4 is important for Na-rich amphibole and is not included in the spreadsheet of Locock (2014). Finally, an all-ferric formula provides the extreme upper $Fe^{3+}/\Sigma Fe$ limit.

MinPlot automatically selects the appropriate lower and upper Fe^{3+} limits. Only one minimum and maximum choice is possible for each analysis. The lower limit is selected as the criterion which gives the minimum normalization factor; however, if all the normalization factors have values greater one, then the ΣFe = Fe^{2+} formula provides the lower limit. Additionally, if the three minima criteria have normalization factors which are lower than those for the four maximum criteria, then Fe^{3+} cannot be estimated and the ΣFe = Fe^{2+} formula is output. In contrast, the maximum normalization factor provides the best estimate for the upper $Fe^{3+}/\Sigma Fe$ limit. After the upper and lower limits are chosen, MinPlot calculates the median composition between these limits (Leake et al. 1997; Hawthorne et al. 2012).

Amphibole analyses are automatically assigned to plots for Ca ($^{B}Ca/^{B}(Ca+Na) \geq 0.75$), Na-Ca ($0.75 > {}^{B}Ca/{}^{B}(Ca+Na) > 0.25$), and Na ($^{B}Ca/^{B}(Ca+Na) \leq 0.25$) groups. The classification scheme of Hawthorne et al. (2012) is used: Amphibole compositions are plotted as $^{C}(Al + Fe^{3+} + 2Ti)$ on the x-axis and $^{A}(Na + K + 2Ca)$ on the y-axis (Figs 4a, c, and S2). There are two problems with this classification, 1. It is very sensitive to the estimated Fe^{3+} content and 2. The compositional space of some common end-member species are not explored (e.g., classification of amphibole as actinolite and riebeckite is not possible). For these reasons, MinPlot includes Si (APFU) vs. X_{Mg} and $Fe^{3+}/(Al + Fe^{3+} + Ti)$ vs. $Fe^{2+}/(Fe^{2+} + Mg + Mn)$ classification plots for Ca-amphiboles and Na-amphiboles, respectively (Fig. 4b, d). Additionally, a plot of ΣFe (APFU) vs $Fe^{3+}/\Sigma Fe$ is available, which can be useful for tracking changes in Fe^{3+} content with overall changes in Fe content. Currently plotting options for orthoamphibole are not available.

3.5. Feldspar

Feldspar (AT_4O_8) is calculated here by normalizing to 8 oxygen equivalents, with A = Ca, Na, K, Ba, Fe^{2+}, Mn, and Mg and T = Al and Si at the tetrahedral site. Endmembers are calculated for anorthite (X_{an} = Ca/(Ca + Na + K)), albite (X_{ab} = Ca/(Ca + Na + K)), and alkali feldspar (X_{or} = K/(Ca + Na + K)). Plotting is available as the classic An-Ab-Or feldspar ternary, with and without subdivisions (Fig. 5). If feldspar subdivisions are selected, the fields for the discredited feldspar intermediate species

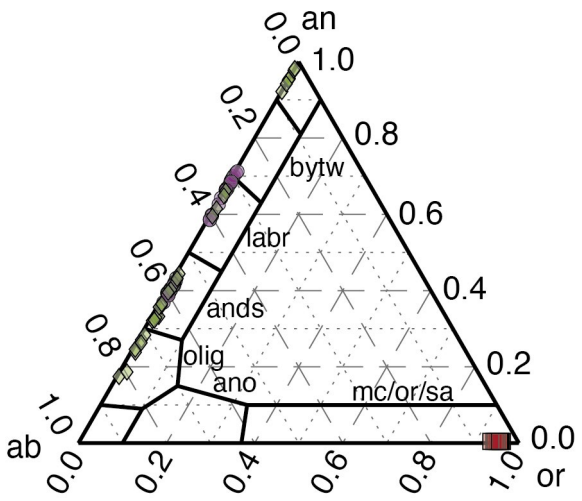


Figure 5. Feldspar anorthite, orthoclase, and albite ternary diagram with compositional subdivisions. Analyses of alkali feldspar (red squares) and plagioclase (purple circles) are from metamorphosed calc silicate rocks from western Maine, USA (SSP18-1A; Walters et al. 2022), as well as plagioclase (green diamonds) from metamorphosed calc silicate rocks from central Nepal (Walters, Kohn 2017).

are plotted: bytownite (bytw, X_{an} = 70-90), labradorite (labr, X_{an} = 70-90), andesine (ands, X_{an} = 30-50), oligoclase (olig, X_{an} = 10-30), and anorthoclase (ano, X_{or}= 10-36). Note that the abbreviations for the intermediate subdivisions are not included in Warr (2021). Boundaries for the feldspar subdivision are commonly drawn either, 1. Maintaining a fixed X_{an} and X_{or}, or 2. Maintaining constant proportion of X_{an}:X_{ab} at varying X_{or} and constant proportion of X_{or}:X_{ab} at varying X_{an}. Here the latter is chosen, and the subdivision boundaries are not parallel to X_{an} and X_{or} (Fig. 5).

3.6. Mica

Mica ($IM_{2\text{-}3}T_4O_{10}W_2$) is calculated here normalizing to 11 oxygen equivalents. Ions are assigned as I = □, K, Na, Ca, and Ba, M = Mg, Mn, Fe^{2+}, Cr, Ti, and ^{VI}Al, T = ^{IV}Al and Si, and W = F, Cl, and OH. While an important I cation in some micas, Li is not considered here as it is not commonly measured. For micas ΣFe is assumed to be Fe^{2+} for the following reasons: 1. Vacancies are possible at both the octahedral and 12-fold coordinated interlayer sites and 2. The estimation of Fe^{3+} by charge balance requires stoichiometric limits to be exceeded, which is rarely the case for micas (Schumacher 1991). Li et al. (2020) proposed a new method of Fe^{3+} estimation of biotite, using a machine learning-based principal component regression; however, Forshaw and Pattison (2021) found a poor fit between observed and predicted Fe^{3+} and Fe^{2+} contents, and the approach is therefore not implemented in MinPlot. It is also important to note that the OH content calculated in MinPlot assumes a full W site (OH = 2 – F – Cl), which may not be accurate and thus provides an estimation of the maximum possible OH content. The OH content is calculated over 50 iterations. Finally, formula recalculation here is calculated normalizing to 11 oxygen equivalents (anhydrous).

Mica endmembers are calculated based on two compositional groups: 1. Dioctahedral muscovite (X_{ms}), ferroceladonite ($X_{Fe\text{-}cel}$), magnesioceladonite ($X_{Mg\text{-}cel}$), paragonite (X_{pg}), margarite (X_{mrg}), and pyrophyllite (X_{prl}) species, or 2. Trioctahedral phlogopite (X_{phl}), annite (X_{ann}), eastonite (X_{eas}), and siderophyllite (X_{sid}) species. The total dioctahedral or trioctahedral components are given as X_{DiOct} and X_{TriOct}, respectively. The calculation procedure is as follows. First, if the sum of the M cations is greater than 2, then some trioctahedral component is possible and is calculated as $X_{TriOct} = \Sigma M - 2$. The total dioctahedral endmembers are then calculated as $X_{DiOct} = 1 - X_{TriOct}$. For dioctahedral micas, first the total fraction (X_M) of muscovite, paragonite, margarite, and pyrophyllite is calculated by scaling ^{VI}Al between 0 and 1, $X_M = {}^{VI}Al - 1$. The total Al-celadonite content (X_{cel}) is then calculated by $X_{cel} = 1 - X_M$. The total celadonite content is then multiplied by the X_{Mg} ratio to calculate the fraction of Fe vs Mg celadonite. Next, the total fraction of muscovite, paragonite, and margarite in X_M is calculated from the APFU of Ca, Na, and K by the equation $X_{ms,pg,mrg} = X_M \cdot (Ca + Na + K)$, whereas the fraction of pyrophyllite is $X_{prl} = 1 - X_{ms,pg,mrg}$. The fractions of muscovite, paragonite, and margarite are then calculated by multiplying $X_{ms,pg,mrg}$ by the ratios of K/(Ca + Na + K), Na/(Ca + Na + K), and Ca/(Ca + Na + K), respectively. Finally, the normalized endmember proportions of the dioctahedral components are calculated by multiplying each by X_{DiOct}, such that the sum of dioctahedral endmembers plus trioctahedral endmembers is unity. For the trioctahedral micas, the total fraction for the phlogopite-annite join is calculated as $X_{phl\text{-}ann}$ = Si - 2 such that individual fractions of phlogopite and annite can be calculated: $X_{phl} = X_{phl\text{-}ann} \cdot X_{Mg}$ and $X_{ann} = X_{phl\text{-}ann} - X_{phl}$. The total fraction for the siderophyllite-eastonite join is also calculated, $X_{sid\text{-}east}$ = 1 - $X_{phl\text{-}ann}$, and the individual fractions for eastonite and siderophyllite are calculated: $X_{east} = X_{sid\text{-}east} \cdot X_{Mg}$ and $X_{sid} = X_{sid\text{-}east} - X_{east}$. Finally, the fractions are normalized such that the proportions of the trioctahedral endmembers and the sum of the dioctahedral endmembers are equal to 1. Plots for micas include the X_{prl}, X_{Alcel}, and X_{ms} ternary (Fig. 6a), celadonite and muscovite + paragonite solid solution diagram (Fig. 6a), Na (APFU) vs. Si (APFU) diagram (Fig. 6c), F-Cl-OH ternary (Fig. 6d), and trioctahedral Ann-Phl-Sid-East solid solution diagram (Fig. 6e). The endmember calculation and plotting schemes proposed here assume simple exchange vectors among endmembers and are useful but remain semi-quantitative.

3.7. Staurolite

Staurolite ($A_4B_4C_{18}D_4T_8O_{40}X_8$) exhibits a complex formula with vacancies on multiple sites: A = Fe^{2+}, Mg, and □, Fe^{2+}, B = Zn, Co, Mg, Li, Al, Fe^{3+},Mn, and □, C = Al, Fe^{3+}, Cr, V, Mg, and Ti, D = Al, Mg, and □, T = Si and Al, and X = OH, Cl, F, and O^{2-} (Hawthorne et al. 1993). Meaningful estimation of Fe^{3+}, OH, and vacancies in the absence of a full quantitative analysis of all elements is not possible. Instead, the composition space is restricted to Mg, Mn, Zn, Fe^{2+}, Fe^{3+}, Al, Ti, and Si. The user may select a ratio for $Fe^{3+}/\Sigma Fe$ before normalization. The values of 0.035 for ilmenite-bearing rocks (X_{hem} < 0.10) and 0.070 for hematite-ilmenite rocks (X_{hem} > 0.10) following Holdaway et al. (1991) are recommended. Normalization is conducted in two ways, 1. Assuming Si + Al = 25.53 APFU following Holdaway et al. (1991) and 2. Normalization to 48 oxygen equivalents. Holdaway et al. (1991) proposed that, following normalization to Si + Al = 25.53 APFU, OH can be estimated by subtracting the sum of the cation charges from 96. If the total OH + F + Cl content is less than 4, the remaining deficit on X is filled by O. If the normalization factor is less than 1, this procedure

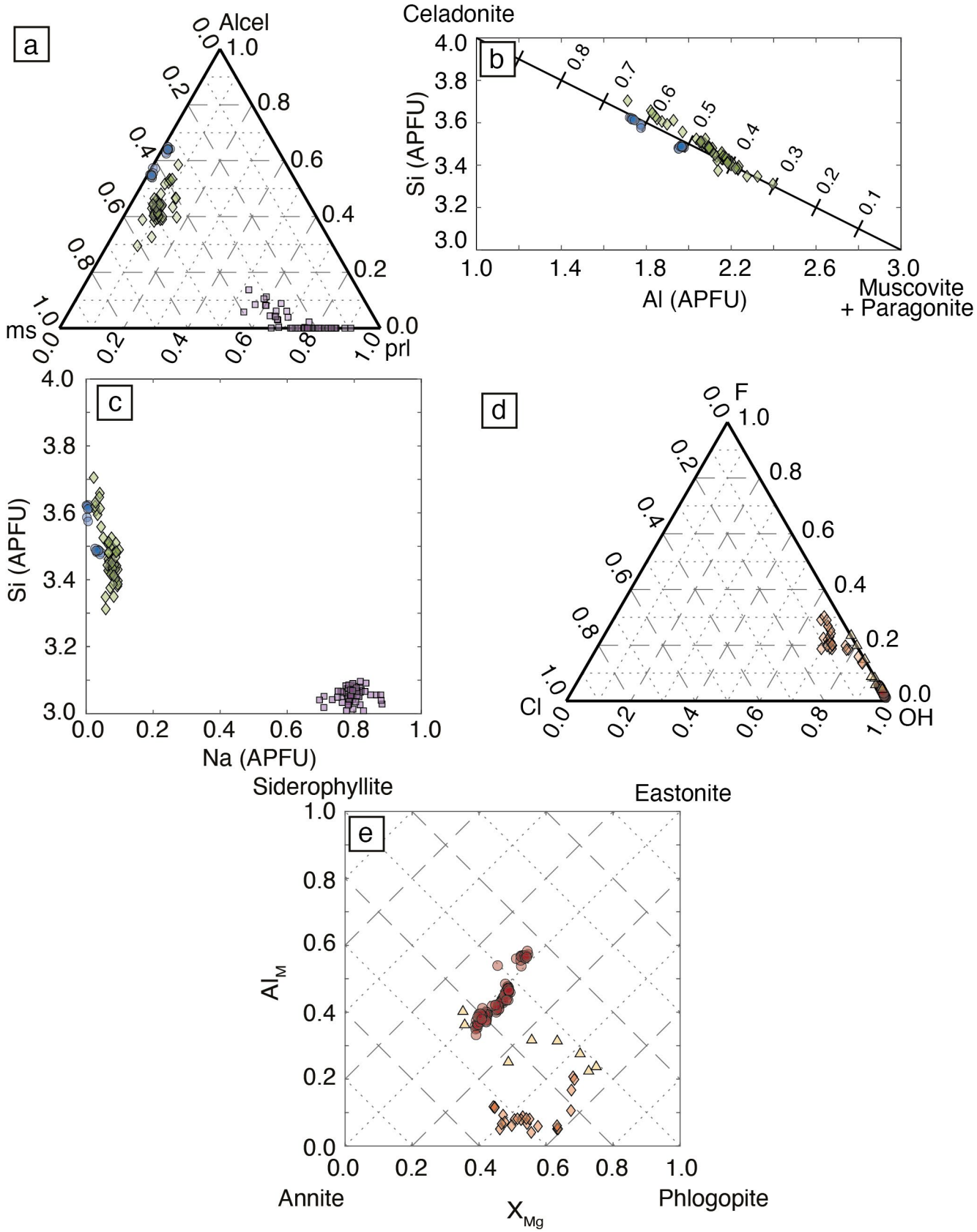


Figure 6. Compositional diagrams for dioctahedral (a–c) and trioctahedral (e) micas: (a) muscovite, celadonite, and pyrophyllite ternary diagram, (b) Al (APFU) vs Si (APFU) diagram showing binary mixing between muscovite + paragonite and celadonite, (c) Na (APFU) vs Si (APFU) diagram, (d) F, OH, and Cl ternary diagram for substitutions on the hydroxyl (W)-site, and (e) X_{Mg} vs Al_M with isolines showing fractional mixing between annite, siderophyllite, eastonite, and phlogopite endmembers. Analyses plotted in (a–c) were collected on phengite (light blue circles) in a blueschist from Port Macquarie, Australia (PMQ065; Walters et al. 2019; 2021), and phengite (green diamonds) and paragonite (purple squares) from an ultrahigh pressure metapelite from the Tian Shan, western China (Xu et al. 2022). Biotite analyses, plotted in (d) and (e), were conducted on grains in a garnet mica schist from western Maine, USA (red circles; Walters et al. 2022), granulite facies para- and orthogneiss from the Larsemann hills, Prydz bay, Antarctica (orange diamonds; Spreitzer et al. 2021), and calc silicate rocks from central Nepal (yellow triangles; Walters, Kohn 2017).

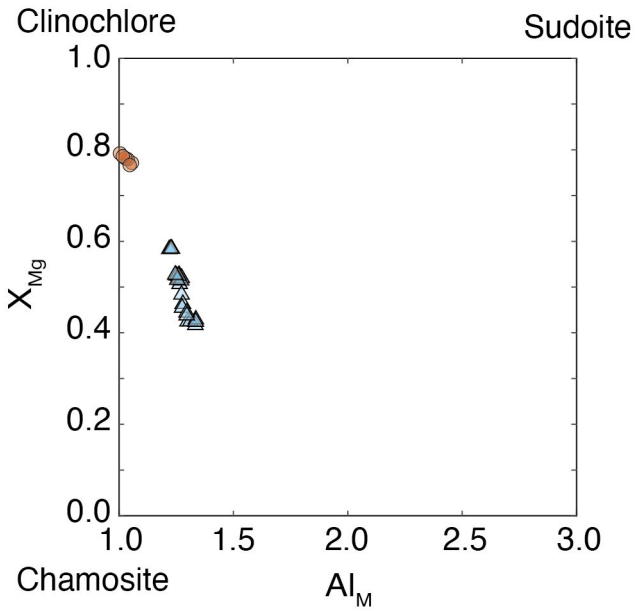


Figure 7. Chlorite compositional diagram with Al_M plotted on the x-axis and X_{Mg} plotted on the y-axis. The compositions of the chamosite, clinochlore, and sudoite endmembers are shown. Analysis of chlorite grains from a chlorite schist black wall sample (SY404) collected on Syros, Greece, are shown as orange circles; whereas, chlorite analyses from a metasomatic garnet-omphacite-chlorite fels (SY462) from the same locality are shown as blue triangles (Walters et al. 2019; 2021).

has the tendency to overfill the anion site (e.g., OH > 4); therefore, the anion sum is an important indicator of the quality of the analysis. Holdaway et al. (1991) estimates an uncertainty of 0.8 APFU (2σ) on the OH estimate using this approach. In both normalization schemes the OH content is refined over 50 iterations. The total number of vacancies is then calculated as vac = 30 - cation total (Holdaway et al. 1991). Further site assignment, endmember calculation, and plotting is not conducted due to the complexity of the structure.

3.8. Cordierite

Cordierite ($A_{0\text{-}1}B_2T2_3T1_6O_{18}$) is calculated here normalized to 18 moles of oxygen equivalents. Cations are assigned as A = Ca, Na, and K, B = Fe^{2+}, Mn, and Mg, T2 = Al and Ti, and T1 = Si and Al. The fraction of magnesium (X_{Mg}) is calculated as Mg/(Mg+Fe). The incorporation of Fe^{3+} is charge balanced by the substitution of Na within the center of the six-membered rings of the cordierite structure (Deer et al. 2013). MinPlot assumes ΣFe = Fe^{2+}, which is not appropriate for rare Na-rich cordierite.

3.9. Chlorite

Chlorite ($M_6T_4O_{10}(OH)_8$) is normalized to 14 oxygen equivalents (anhydrous). Cations are assigned as M = Mg, Mn, Fe^{2+}, Ni, Ti, ^{VI}Al, and □ at the octahedral site, whereas T = ^{IV}Al and Si at the tetrahedral site. Vacancies on M1 are calculated by □ = 0.5(^{VI}Al - ^{IV}Al) following Lanari et al. (2014b). In low-Fe chlorite, Fe^{3+} substitution may be dominantly the result of exchange with Al, resulting in a fictive 'Fe^{3+}-rich Mg-amesite' endmember (Masci et al. 2019). Second, the exchange vector $^{VI}\square + 2^{VI}R^{3+} = 3\,^{VI}(Mg,Fe^{2+})$ may induce vacancies where R^{3+} is Al or Fe^{3+}. Masci et al. (2019) show that a third substitution, following the exchange vector (Fe^{2+}, Mg) + H^+ = Fe^{3+}, may be the primary mechanism behind elevated Fe^{3+} in Fe-rich chlorite. It is possible that other elements, such as Al or Cr, may also substitute via deprotonation. As a result, fully quantitative structural assignment and endmember determination requires the direct analysis of Fe^{3+}, as well as OH and/or O_2. These structural complexities preclude Fe^{3+} estimation by charge balance, and here MinPlot assumes ΣFe = Fe^{2+}.

Chlorite compositions are plotted in a diagram of ^{VI}Al vs X_{Mg}, which explores the compositional space between the clinochlore, chamosite, and sudoite endmembers (Fig. 7). Like micas, the chlorite compositional plot assumes simple exchange vectors and does not explore the full compositional space or account for Fe^{3+}, which may be significant in some chlorite. Nevertheless, the plot is useful monitor for compositional variability.

3.10. Chloritoid

Chloritoid is made up of two octahedral layers, L1 and L2, linked by SiO_4 tetrahedra, where L1 is (Na, Ca, Mg, Mn, Fe^{2+})$_2$(Al,Ti,Fe^{3+})$O_2(OH)_4$, L2 is Al_3O_2, and the tetrahedral (*T*) site is 2[SiO_4]. Here Fe^{3+} is estimated by charge balance criteria. At low Fe^{3+}, the OH site is close to filled, but may be less than the ideal sum in Fe^{3+}-rich chlorit-

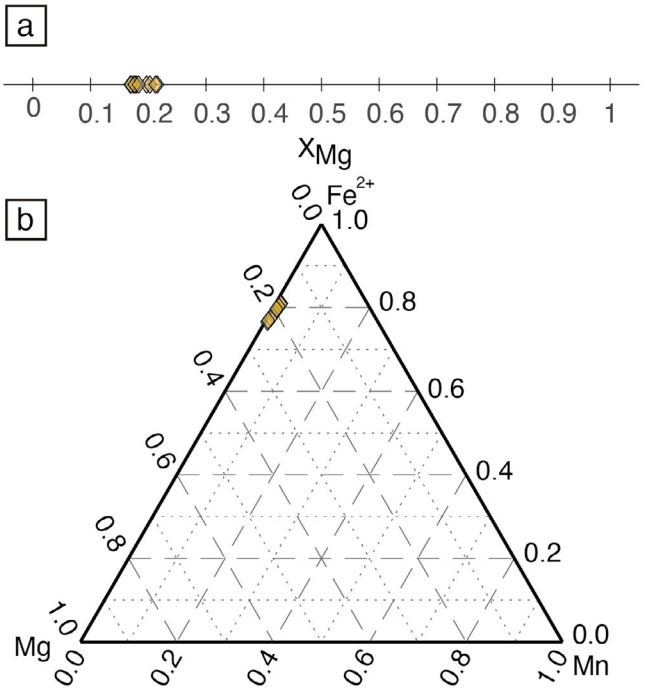


Figure 8. (a) Binary X_{Mg} and (b) ternary Fe^{2+}, Mg, and Mn compositional diagrams for chloritoid. Analytical data were collected on chloritoid inclusions in garnet cores in eclogite from As Sifah, Oman (Unpublished).

oid, consistent with deprotonation and oxidation of Fe^{2+} to Fe^{3+} (Deer et al. 2013). While the assumption of 8 cations and 12 oxygen equivalents (anhydrous) used here to calculate Fe^{3+} is violated at elevated Fe^{3+} (which may occupy up to 50% of R^{3+} in the L1 layers), such high Fe^{3+} chloritoid compositions are rare (Deer et al. 2013). The calculation procedure used here is expected to perform well for most chloritoid analyses. Chloritoid compositions may be plotted as either a X_{Mg} binary (with adjustable upper and lower limits) or in the Fe^{2+}-Mg-Mn ternary (Fig. 8).

3.11. Talc

The structural formula for talc ($M_3T_4O_{10}(OH)_2$) is normalized here to 11 oxygen equivalents (anhydrous), with M = K, Na, Ca, Mg, Mn, Fe^{2+}, Ni, Ti, and ^{VI}Al allocated to the octahedral site, and T = ^{IV}Al and Si at the tetrahedral site. Here ΣFe is assumed to be Fe^{2+}. Compositional plots are not currently offered.

3.12. Epidote group

Compositions of epidote group members are described as $A_2M_3T_3(O,OH,F)_{12}$, where A = K, Na, Ca, and Mg, M = Mn^{3+}, Fe^{3+}, Cr, Ti, and ^{IV}Al, and T = ^{IV}Al and Si. The most abundant epidote group minerals fall between the (clino-)zoisite ($Ca_2Al_3Si_3O_{11}O(OH)$) and epidote ($Ca_2Al_2Fe^{3+}Si_3O_{11}O(OH)$) endmembers. While the exchange vectors with piemontite ($Ca_2Al_2Mn^{3+}Si_3O_{11}O(OH)$) and Cr-epidote ($Ca_2Al_2CrSi_3O_{11}O(OH)$) are considered here, the substitutions of Ce, Sr, Pb, La, Y and Th at A are not currently implemented in MinPlot. All Fe and Mn are assumed to be trivalent. Normalization is based on a 12.5 oxygen equivalent (anhydrous) basis. Endmember fractions are expressed as (clino-)zoisite (X_{czo} = (Al^{VI} - 2)/(Fe^{3+} + Al^{VI} + Cr + Mn^{3+} - 2)), epidote (X_{ep} = Fe^{3+}/(Fe^{3+} + Al^{VI} + Cr + Mn^{3+} - 2)), piemontite (X_{pmt} = Mn^{3+}/(Fe^{3+} + Al^{VI} + Cr + Mn^{3+} - 2)), and Cr-epidote (X_{Crep} = Cr/(Fe^{3+} + Al^{VI} + Cr + Mn^{3+} - 2). Epidote compositions are plotted in an Al-Fe^{3+} binary diagram, like plots offered for olivine (Fig. 3a) and chloritoid (Fig. 8a).

3.13. Titanite

Titanite ($CaTiSiO_5$) has three structural sites and may display significant compositional variability. The 7-fold decahedral site may incorporate K, Na, Y, and Ca, the octahedral site may incorporate Mg, Mn, Fe^{3+}, Ti, and ^{VI}Al, and the tetrahedral site contains Si and ^{IV}Al. Rare Earth elements, Sr, Pb, and U may also substitute into the decahedral site, as well as Zr, Nb, and Ta on the octahedral site, but are not considered here due to their relatively low abundance in most titanite. Here, all Fe is considered as Fe^{3+} and titanite analyses are normalized to fully occupied octahedral and tetrahedral sites:

$$NF^C = \frac{2}{\sum_i^Z n_{Oct}^C + \sum_i^Z n_T^C} \quad (10)$$

Where NF^C is the cation-based normalization factor, $\sum_i^Z n_{Oct}^C$ is the sum of Mg, Mn, Fe^{3+}, Ti, and Al^{VI}, and $\sum_i^Z n_T^C$ is the sum of Si and Al^{IV}. Fluorine and OH^- are thought to substitute for O via the exchange vector $(Al,Fe)^{3+} + (OH,F)^- = Ti^{4+} + O^{2-}$ (see review in Kohn 2017). Fluorine may be measured by directly EPMA; whereas, OH is calculated as OH = (Al^{VI} + Fe^{3+}) - F. Oxygen is calculated as the sum of the cation charges minus 0.5(F + OH). Finally, the fraction of titanite is calculated as X_{ttn} = Ti/ $\sum_i^Z n_{Oct}^C$. Currently no plotting options are available for titanite.

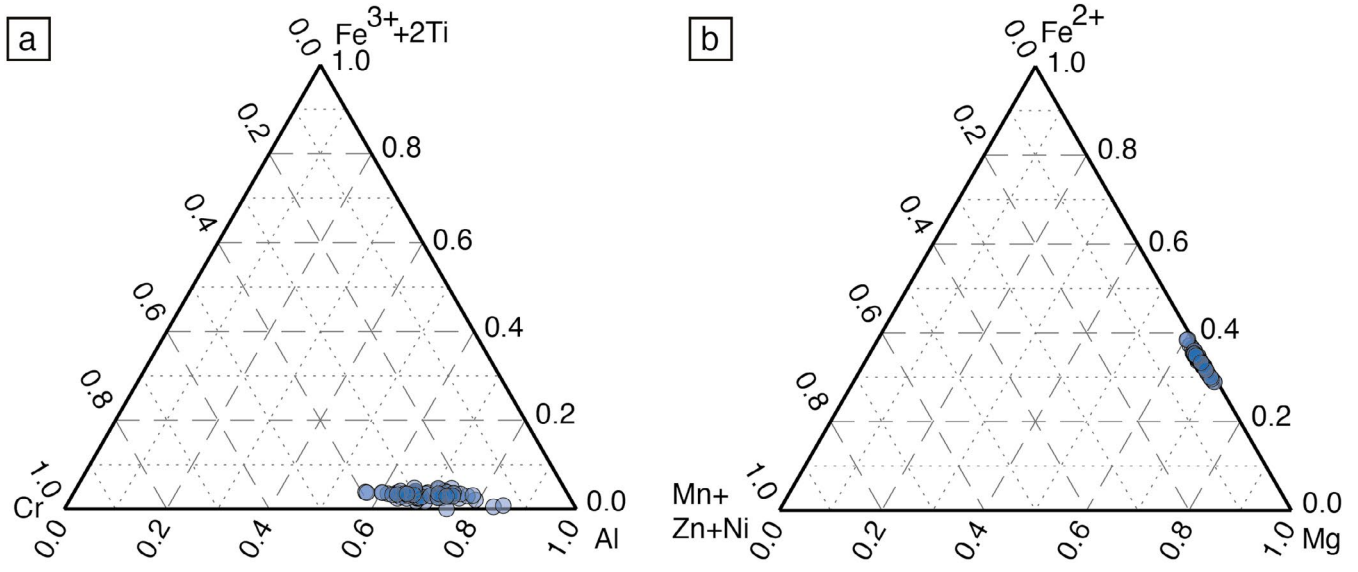


Figure 9. Ternary (a) Fe^{3+} + 2Ti, Al, and Cr and (b) Fe^{2+}, Mg, and Mn + Zn + Ni diagrams for spinel. Data are analyses of spinel from mantle peridotite, Wadi Fins, Oman (de Obseso, Kelemen 2020).

3.14. Oxyspinel

Oxyspinel group minerals ($A^{2+}B_2^{3+}O_4$) are calculated here to 3 cations and 4 oxygen equivalents for Fe^{3+} estimation. Here A = Mg, Mn, Fe^{2+}, Zn, and Ni at the tetrahedral site, whereas B = Fe^{3+}, Cr, Al, and Ti at the octahedral site. Oxyspinel compositions are plotted in the Cr, Fe^{3+} + 2Ti, and Al and Fe^{2+}, Mg, and Mn + Zn + Ni ternary diagrams (Fig. 9a, b, respectively).

3.15. Sulfides

A generic procedure is available for sulfide minerals. The datafile requires the mass fractions (in wt%) for S, Co, Cu, As, Fe, Ni, Pb, and Zn. All elements, except for S, are optional, allowing the maximum flexibility for a variety of sulfides. There are multiple options for normalization. First, the user is asked to specify if they want to normalize on a cation or anion basis. Cation normalization works well for many sulfides but should not be done for pyrrhotite ($Fe_{1-X}S$) where the cation total is not fixed. Second, As (–3 to +5) can be treated either as a cation or an anion. On the reduced end As^{1-} may substitute as an anion in pyrite and other disulfides. However, at more oxidizing conditions As^{2+} and As^{3+} may substitute for divalent and trivalent cations (e.g., Deditus et al. 2008; Qian et al. 2013). Trends in Fe-As-S ternary space may be used to determine whether As should be treated as a cation or anion for a given analysis (e.g., Deditus et al. 2014). Currently no compositional diagrams are available for sulfide phases.

4. Additional considerations

MinPlot is intended to process and plot EPMA data. Corrections for matrix effects, such as absorption and fluorescence, must be made prior to using MinPlot. Additionally, MinPlot does not filter or label substandard analyses. MinPlot does not automatically identify the phase of interest and select the appropriate recalculation method. Instead, the user is required to identify the mineral species analyzed prior to use of the program. In both cases, the calculated site (or group) fractions and sums can be used to determine whether the correct calculation scheme was used or if the data is of high quality. In the case of Fe^{3+}-Fe^{2+} determination by stoichiometry, the oxygen deficiency (which must be >0, but is generally << 1) is useful for identifying poor quality or misidentified analyses. In particular, special care must be taken for evaluating the Fe^{3+}-Fe^{2+} estimation for amphibole, where certain upper and lower Fe^{3+} estimation criteria may be inappropriate for some compositions. Importantly, MinPlot is not intended to replace traditional manual recalculation of mineral formulae for educational purposes. There are numerous educational resources for users who are new to mineral formula recalculation, such as the appendix of Deer et al. (2013) for the general approach and Schumacher (1991) and Droop (1987) for Fe^{3+}-Fe^{2+} estimation procedures.

Users should keep in mind that, where offered, endmember fractions are estimates that are calculated over a restricted compositional space. Such fractions are useful for comparison between or within samples but are subject to systematic inaccuracies. For example, the garnet supergroup contains 32 approved species at the time of writing of Grew et al. (2013); whereas, here the compositional space of garnet endmember fractions is restricted to five species. These restrictions are not entirely arbitrary: Most garnet crystals can be described within the considered compositional space. However, even within the chosen compositional space, endmembers may exist that are not considered, but are a linear combination of the composition of other endmembers. For example, the garnet endmember calderite ($Mn_3^{2+}Fe_2^{3+}Si_3O_{12}$), which is not calculated in MinPlot, can be described as a linear combination of the endmembers pyrope plus andradite minus grossular. While the restriction of the compositional space to the elements Fe^{2+}, Fe^{3+}, Ca, Mg, Mn^{2+}, Al, and Cr is not arbitrary, as it covers the most common garnet compositions, the choice of endmembers within that space is arbitrary, such as choosing andradite as the Fe^{3+} endmember over calderite. In the case of minerals with very large complex composition spaces (e.g., more than 4-5 dimensions), such as amphibole, it makes little mathematical sense to report endmember fractions, and this is not done here.

Finally, empirical and theoretical major element thermobarometers commonly utilize endmember fractions or site fractions to calculate pressure and temperature from EPMA analyses of natural minerals. The composition space considered for these thermobarometers is regularly simplified, commonly due to the difficulty of developing activity-composition relationships from fits to experimental and natural data (see review in Lanari and Duesterhoeft 2019). The calculation procedures in MinPlot do not make the same assumptions and are not directly comparable. Additionally, many minerals display ordering of the same elements across multiple crystallographic sites. For example, C cations in amphibole, such as Fe and Mg, may occur at the *M*1, *M*3, and *M*4 sites. Order-disorder involves the preference or non-preference of these elements for *M*1, *M*3, or *M*4, in this case. Many thermobarometers assume equipartitioning (a random distribution), such that the relative fractions of the cations (e.g., X_{Mg}) is preserved on each site. However, equipartitioning assumes full disorder, which is usually not correct, and instead a thermodynamic approach is required to determine the correct ordering at a known pressure and temperature (see discussion

in Holland and Powell 2006). Here, equipartitioning is not assumed for most minerals. For amphibole, as an example, C cations are not further assigned to *M*1, *M*3, or *M*4 sites. For these reasons, MinPlot output should not be used in thermodynamic calculations. Instead, users should use normalization, site assignment, and endmember fraction calculation procedures that match exactly those used to calibrate the thermobarometer and/or activity-composition model considered in thermodynamic calculations. For example, XMapTools offers mineral formula recalculation from quantified X-ray maps that are consistent with the calibrations of the thermobarometers implemented in the program (Lanari et al. 2014; 2019). Instead, MinPlot serves a different purpose, to recalculate mineral formulae meaningfully and accurately for the purpose of plotting chemical trends and classifying mineral compositions.

5. Conclusions

Electron probe microanalysis is a powerful tool for measuring raw contents of major and minor elements in geological materials; however, the identification of geologically important compositional trends requires formula recalculation of the raw EPMA data. MinPlot is a MATLAB®-based program, which runs on a central script that calls multiple recalculation and plotting procedures for 15 mineral groups. Due to the modular nature of MinPlot, adding additional functions for new minerals is simple, allowing the program to be easily modified and updated to include new minerals and data visualization procedures. MinPlot is also anticipated to be compatible with future releases of MATLAB®; whereas, many older mineral formula recalculation programs are no longer in use because they are unsupported on modern operating systems. Finally, MinPlot provides publication ready compositional plots for most common minerals. By coding MinPlot using the MATLAB® programming language, the user is required to have a license; however, a future standalone or web-based application is planned.

6. Code Availability

The MinPlot program, source code, and data files used to make the figures in this manuscript are hosted in a GitHub repository (https://github.com/MinPlot). Future updates will be posted here and past versions of MinPlot archived.

Acknowledgements

MinPlot would not have been possible without a lot of help along the way. I sincerely thank Martin Yates, Heidi Höfer, Dominik Hezel, Christopher Mattinson, and Mike Dorias for their guidance and training on the EPMA over the years. I would also like to thank Edward S. Grew, Horst R. Marschall, John Schumacher, Guillaume Bonnet, Guillaume Siron, and many others for their helpful and interesting discussions on mineral chemistry and mineral formula recalculation. Pierre Lanari, John Schumacher, and Łukasz Kruszewski are thanked for their throughout and insightful reviews of this manuscript. Jarosław Majka is also thanked for his editorial handling of the manuscript.

Conflicts of interest

The author has no conflicts of interest to declare.

Supplementary Material

Supplementary data to this article can be found online at https://doi.org/10.2478/mipo-2022-0005.

References

Afifi, A.M., & Essene, E. (1988). MINFILE: A microcomputer program for storage and manipulation of chemical data on minerals. *American Mineralogist*, *73*, 446-448.

Bernhardt, H.J. (2010). MINCALC-V5, a non EXCEL based computer program for general electron-microprobe mineral analyses data processing. *IMA 20th General Meeting 2010, Acta Mineralogy and Petrology Abstract Series*, *6*, 869.

Brandelik, A. (2009). CALCMIN – an EXCELTM Visual Basic application for calculating mineral structural formulae from electron microprobe analyses. *Computers & Geosciences, 35*, 1540-1551. DOI: 10.1016/j.cageo.2008.09.011.

De Angelis, S.M.H., & Niell, O.K. (2012). MINERAL: A program foor the propagation of analytical uncertainty through mineral formula recalculations. *Computers & Geosciences, 48*, 134-142. DOI: 10.1016/j.cageo.2012.05.023.

Deditius, A.P., Reich, M., Kesler, S.E., Utsunomiya, S., Chryssoulis, S.L., Walshe, J., & Ewing, R.C. (2014). The coupled geochemistry of Au and As in pyrite from hydrothermal ore deposits. *Geochimica et Cosmochimica Acta*, *140*, 644-670. DOI: 10.1016/j.gca.2014.05.045.

Deditius, A.P., Utsunomiya, S., Renock, D., Ewing, R.C., Ramana, C.V., Becker, U., & Kesler, S.E. (2008). A proposed new type of arsenian pyrite: Composition, nanostructure and geological significance. *Geochimica et Cosmochimica Acta*, *72*, 2919-2933. DOI: 10.1016/j.gca.2008.03.014.

De Bjerg, S.C., Mogessie, A., & Bjerg, E. (1992). HYPER-FORM – A Hypercard® program for Macintosh® microcomputers to calculate mineral formulae from electron microprobe and wet chemical analysis. *Computers & Geosciences, 30*, 909-923. DOI: 10.1016/0098-3004(92)90006-D.

De Bjerg, S.C., Mogessie, A., & Bjerg, E. (1995). PASFORM – A program for IBM® PC or PC-compatible computers to calculate mineral formulae from electron microprobe and wet-chemical analysis. *Computers & Geosciences, 21*, 1187-1190. DOI: 10.1016/0098-3004(95)00049-6.

Deer, W.A., Howie, R.A., & Zussman, J. (2013). *An introduction to the rock-forming minerals* (3 ed.). London: Mineralogical Society of Great Britain and Ireland. DOI: 10.1180/DHZ.

De Obeso, J.C., & Kelemen, P.B. (2020). Major element mobility during serpentinization, oxidation and weathering of mantle peridotite at low temperatures. *Philosophical Transactions of the Royal Society A*, *378*, 20180433. DOI: 10.1098/rsta.2018.0433.

Droop, G.T.R. (1987). A general equation for estimating Fe^{3+} concentrations in ferromagnesian silicates and oxides from microprobe analysis, using stoichiometric criteria. *Mineral Magazine*, *51*, 431-437.

Esawi, E.K. (2004). AMPH-CLASS: An Excel spreadsheet for the classification and nomenclature of amphiboles based on the 1997 recommendations of the International Mineralogical Association. *Computers and Geosciences, 30*, 753-760. DOI: 10.1016/j.cageo.2004.05.007.

Forshaw, J.B., & Pattison, D.R.M. (2021). Ferrous/ferric (Fe^{2+}/Fe^{3+}) partitioning among silicates in metapelites. *Contributions to Mineralogy and Petrology, 176*, 1-26. DOI: 10.1007/s00410-021-01814-4.

Grew, E.S., Locock, A.J., Mills, S.J., Galuskina, I.O., Galuskin, E.V., & Hålenius, U. (2013). Nomenclature of the garnet supergroup. *American Mineralogist*, *98*, 785-811. DOI: 10.2138/am.2013.4201.

Hawthorne, F.C., Oberti, R., Harlow, G.E., Maresch, W.V., Martin, R.F., Schumacher, J.C., & Welch, M.D. (2012). Nomenclature of the amphibole supergroup. *American Mineralogist*, *97*, 2031-2048. DOI: 10.2138/am.2012.4276.

Hawthorne, F.C., Ungaretti, L., Oberti, R., Caucia, F., & Callegari, A. (1993). The crystal chemistry of staurolite. I. Crystal structure and site populations. *The Canadian Mineralogist*, *31*, 551-582.

Harlow, G.E. (1999). Interpretation of Kcpx and CaEs components in clinopyroxene from diamond inclusions and mantle samples. Proceedings of the 7th *International Kimberlite Conference*, *1*, 321-331.

Holdaway, M.J., Mukhopadhyay, B., Dyar, M.D., Dutrow, B.L., Rumble, D., & Grambling, J.A. (1991). A new perspective on staurolite crystals chemistry: Use of stoichiometric and chemical end-members for a mole fraction model. *American Mineralogist*, *76*, 1910-1991.

Knowles, C.R. (1987). A BASIC program to recast garnet end-members. *Computers & Geosciences*, *13*, 655-659.

Kohn, M.J. (2017). Titanite petrochronology. *Reviews in Mineralogy and Geochemistry*, *83*, 419-441. DOI: 10.2138/rmg.2017.83.13.

Lanari, P., Vidal, O., de Andrade, V., Dubacq, B., Lewin, E., Grosch, E.G., & Schwartz, S. (2014a). XMapTools: A MATLAB®-based program for electron microprobe X-ray image processing and geothermobarometry. *Computers & Geosciences*, *62*, 227-240. DOI: 10.1016/j.cageo.2013.08.010.

Lanari, P., Wagner, T., & Vidal, O. (2014b). A thermodynamic model for di-trioctahedral chlorite from experimental and natural data in the system MgO-FeO-Al_2O_3-SiO_2-H_2O: Applications to *P–T* sections and geothermometry. *Contributions to Mineralogy and Petrology*, *167*(968), 1-19. DOI: 10.1007/s00410-014-0968-8.

Lanari, P., Vho, A., Bovay, T., Airaghi, L., & Centrella, S. (2019). Quantitative compositional mapping of mineral phases by electron probe micro-analyser. *Geological Society of London, Special Publications*, *478*, 39-63. DOI: 10.1144/SP478.4.

Leake, B.E., Woolley, A.R., Arps, C.E.S., Birch, W.D., Gilbert, M.C., Grice, J.D., Hawthorne, F.C., Kato, A., Kish, H.J., Krivovichev, V.G., Linthout, K., Laird, J., Mandarino, J.A., Maresch, W.V., Nickel, E.H., Rock, N.M.S., Schumacher, J.C., Smith, D.C., Stephenson, N.C.N., Ungaretti, L., Whittaker, E.J.W., & Youzhi, G. (1997). Nomenclature of amphiboles: Report of the subcommittee on amphiboles of the International Mineralogical Association, Commission on New Minerals and Mineral Names. *The Canadian Mineralogist*, *35*, 219-246.

Li, X., Zhang, C., Behrens, H., & Holtz, F. (2020). Calculating biotite formula from electron microprobe analysis data using a machine learning method based on principal components regression. *Lithos, 356-357*: 105371. DOI: 10.1016/j.lithos.2020.105371.

Le Pioufle, A., & Canil, D. (2012). Iron in monticellite as an oxygen barometer for kimberlite magmas. *Contributions to Mineralogy and Petrology*, *163*, 1033-1046. DOI: 10.1007/s00410-011-0714-4.

Locock, A.J. (2008). An Excel spreadsheet to recase analyses of garnet into end-member components, and a synopsis of the crystal chemistry of natural silicate garnets. *Computers & Geosciences*, *34*(12), 1769-1780. DOI: 10.1016/j.cageo.2007.12.013.

Locock, A.J. (2014). An Excel spreadsheet to classify chemical analyses of amphibole following the IMA 2012 recommendations. *Computers & Geosciences*, *62*, 1-11. DOI: 10.1016/j.cageo.2013.09.011.

Masci, L., Dubacq, B., Verlaguet, A., Chopin, C., de Andrade, V., & Herviou, C. (2019). A XANES and EPMA study of Fe^{3+} in chlorite: Importance of oxychlorite and implications for cation site distribution and thermobarometry. *American Mineralogist*, *104*, 403-417. DOI: 10.2138/am-2019-6766.

Meija, J., Coplen, T.B., Berglund, M., Brand, W.A., De Bièvre, P., Gröning, M., Holden, N.E., Irrgeher, J., Loss, R.D., Walczyk, T., & Prohaska, T. (2016). Atomic weights of the elements 2013 (IUPAC Technical Report). *Pure and Applied Chemistry*, *88*, 265-291. DOI: 10.1515/pac-2015-0305.

Mogessie, A., Tessadri, R., & Veltman, C.B. (1990). EMP-AMPH – a Hypercard program to determine the name of an amphibole from electron microprobe analysis according to the International Mineralogical Association scheme. *Computers and Geosciences*, *16*, 309-330. DOI: 10.1016/0098-3004(90)90066-3.

Mogessie, A. (2001). AMPH-IMA97: a Hypercard program to determine the name of an amphibole from electron microprobe and wet chemical analyses. *Computers and Geosciences*, *27*, 1171-1180. DOI: 10.1016/S0098-3004(01)00034-6.

Morimoto, N., Fabries, J., Ferguson, A.K., Ginzburg, I.V., Ross, M., Seifert, F.A., Zussman, J., Aoki, K., & Gottardi, G. (1989). Nomenclature of pyroxenes. *Mineralogical Magazine*, *52*, 535-550. DOI: 10.1180/minmag.1988.052.367.15.

Oberti, R., Ungretti, L., Cannnillo, E., & Hawthorne, F.C. (1992). The behaviour of Ti in amphiboles. I. Four- and six-coordinate Ti in richterite. *European Journal of Mineralogy*, *4*, 425-439.

Piccardo, G.B., & Guarnieri, L. (2011). Gabbro-norite cumulates from strongly depleted MORB melts in the Alpine-Apennine ophiolites. *Lithos*, *124*, 200-214. DOI: 10.1016/j.lithos.2011.01.017.

Qian, G., Brugger, J., Testemale, D., Skinner, W., & Pring, A. (2013). Formation of As(II)-pyrite during experimental replacement of magnetite under hydrothermal conditions. *Geochimica et Cosmochimica Acta*, *100*, 1-10. DOI: 10.1016/j.gca.2012.09.034.

Rao, D.R., & Rao, T.V.S. (1996). AMPH: A program for calculating formulae for assigning names to the amphibole group of minerals. *Computers & Geosciences*, *22*, 931-933. DOI: 10.1016/S0098-3004(96)00018-0.

Richard, L.R., & Clarke, D.B. (1990). AMPHIOBOL: A program for calculating structural formulae and for classifying and plotting chemical analyses of amphiboles. *American Mineralogist*, *75*, 421-423.

Rock, N.M.S., & Carroll, G.W. (1990). MINTAB: A general-purpose mineral recalculation and tabulation program for Macintosh. *American Mineralogist*, *75*, 424-430.

Rock, N.M.S. (1987). A FORTRAN program for tabulating and naming amphibole analyses according to the International Mineralogical Association scheme. *Mineralogy and Petrology*, *37*, 79-88. DOI: 10.1007/BF01163159.

Rock, N.M.S., & Leake, R.E. (1984). The International Mineralogical Association amphibole nomenclature scheme: Computerization and its consequences. *Mineralogical Magazine*, *48*, 211-227.

Schumacher, J.C. (1991). Empirical ferric iron corrections: Necessity, assumptions, and effects on selected geothermobarometers. *Mineralogical Magazine*, *55*, 3-18. DOI: 10.1180/minmag.1991.055.378.02.

Spear, F.S., & Kimball, K.L. (1984). RECAMP – A FORTRAN IV program for estimating Fe^{3+} contents in amphiboles. *Computers in Geology*, *10*, 317-325. DOI: 10.1016/0098-3004(84)90029-3.

Spreitzer, S.K., Walters, J.B., Cruz-Uribe, A.M., Williams, M.L., Yates, M.G., Jercinovic, M.J., Grew, E.S., & Carson, C.J. (2021). Monazite petrochronology of polymetamorphic granulite-facies rocks of the Larsemann Hills, Prydz Bay, East Antarctica. *Journal of Metamorphic Geology*, *39*, 1205-1228. DOI: 10.1111/jmg.12607.

Sturm, R. (2002). PX-NOM – An interactive spreadsheet program for the computation of pyroxene analyses derived from the electron microprobe. *Computers & Geosciences*, *28*, 473-483. DOI: 10.1016/S0098-3004(01)00083-8.

Tiepolo, M., Zanetti, A., & Oberti, R. (1999). Detection, crystal-chemical mechanisms and petrological implications of $^{[6]}Ti^{4+}$ partitioning in pargasite and kaersutite. *European Journal of Mineralogy*, *11*, 345-354. DOI: 10.1127/ejm/11/2/0345.

Tindle, A.G., & Webb, P.C. (1994). Probe-AMPH – A spreadsheet program to classify microprobe-derived amphibole analyses. *Computers & Geosciences*, *20*, 1201-1228. DOI: 10.1016/0098-3004(94)90071-X.

Xu, J., Zhang, G.B., Marschall, H.R., Walters, J.B., Liu, S.Q., Lü, Z., Zhang, L.F., Hu, H., & Li, N. (2022). Boron isotopes of white mica and tourmaline in an ultra-high pressure metapelite from the western Tianshan, China: Dehydration and metasomatism during exhumation of subducted ocean-floor sediments. *Contributions to Mineralogy and Petrology*, *177*(46), 1-16. DOI: 10.1007/s00410-022-01916-7.

Yavuz, F. (2003a). Evaluating micas in petrologic and metallogenic aspect: I – definitions and structure of the computer program MICA+. *Computers & Geosciences*, *29*, 1203-1213. DOI: 10.1016/S0098-3004(03)00142-0.

Yavuz, F. (2003b). Evaluating micas in petrologic and metallogenic aspect: II – applications using the computer program MICA+. *Computers & Geosciences*, *29*, 1215-1228. DOI: 10.1016/S0098-3004(03)00143-2.

Yavuz, F. (2007). WinAmphcal: A windows program for the IMA-04 amphibole classification. *Geochemistry, Geophysics, Geosystems*, *8*, Q01004. DOI: 10.1029/2006GC001391.

Yavuz, F. (2013). WinPyrox: A Windows program for pyroxene calculation classification and thermobarometry. *American Mineralogist, 98*, 1338-1359. DOI: 10.2138/am.2013.4292.

Yavuz, F., Kumral, M., Karakaya, N., Karakaya, M.C., & Yildirim, D.K. (2015). A windows program for chlorite calculation and classification. *Computers & Geosciences*, *81*, 101-113. DOI: 10.1016/j.cageo.2015.04.011.

Yavuz, F., & Yildirim, D.K. (2020). WinGrt, a Windows program for garnet supergroup minerals. *Journal of Geosciences*, *65*, 71-95. DOI: 10.3190/jgeosci.303.

Walters, J.B., Cruz-Uribe, A.M., & Marschall, H.R. (2019). Isotopic compositions of sulfides in exhumed high-pressure terranes: Implications for sulfur cycling in subduction zones. *Geochemistry, Geophysics, Geosystems*, *20*, 2019GC008374. DOI: 10.1029/2019GC008374.

Walters, J.B., Cruz-Uribe, A.M., Marschall, H.R., & Boucher, B. (2021). The role of sulfides in the chalcophile and siderophile element budget of the subducted oceanic crust. *Geochimica et Cosmochimica Acta*, *304*, 191-215. DOI: 10.1016/j.gca.2021.04.016.

Walters, J.B., Cruz-Uribe, A.M., Song, W.J., Gerbi, C., & Biela, K. (2022). Strengths and limitations of in situ U-Pb titanite petrochronology in polymetamorphic rocks: An example from western Maine, USA. *Journal of Metamorphic Geology*, *40*, 1043-1066. DOI: 10.1111/jmg.12657.

Walters, J.B., & Kohn, M.J. (2017). Protracted thrusting followed by late rapid cooling of the Greater Himalayan Sequence, Annapurna Himalaya, Central Nepal: Insights from titanite petrochronology. *Journal of Metamorphic Geology*, *35*, 897-917. DOI: 10.1111/jmg.12260.

Warr, L.N. (2021). IMA-CNMNC approved mineral symbols. *Mineralogical Magazine, 85*, 291-320. DOI: 10.1180/mgm.2021.43.

Received: 01 Aug 2022
Accepted: 11 Nov 2022
Handling Editor: Jarosław Majka